JCTC Journal of Chemical Theory and Computation

pubs.acs.org/JCTC Article

On the Interplay between Electronic Structure and Polarizable Force Fields When Calculating Solution-Phase Charge-Transfer Rates

Jaebeom Han, Pengzhi Zhang, Huseyin Aksu, Buddhadev Maiti, Xiang Sun,* Eitan Geva,* Barry D. Dunietz,* and Margaret S. Cheung*

Cite This: *J. Chem. Theory Comput.* 2020, 16, 6481−6490 Read Online

ACCESS | Metrics & More | Article Recommendations | Supporting Information

ABSTRACT: We present a comprehensive analysis of the interplay between the choice of an electronic structure method and the effect of using polarizable force fields vs. nonpolarizable force fields when calculating solution-phase charge-transfer (CT) rates. The analysis is based on an integrative approach that combines inputs from electronic structure calculations and molecular dynamics simulations and is performed in the context of the carotenoid−porphyrin−C_{60} molecular triad dissolved in an explicit tetrahydrofuran (THF) liquid solvent. Marcus theory rate constants are calculated for the multiple CT processes that occur in this system based on either polarizable or nonpolarizable force fields, parameterized using density functional theory (DFT) with either the B3LYP or the Baer−Neuhauser−Livshits (BNL) density functionals. We find that the effect of switching from nonpolarizable to polarizable force fields on the CT rates is strongly dependent on the choice of the density functional. More specifically, the rate constants obtained using polarizable and nonpolarizable force fields differ significantly when B3LYP is used, while much smaller changes are observed when BNL is used. It is shown that this behavior can be traced back to the tendency of B3LYP to overstabilize CT states, thereby pushing the underlying electronic transitions to the deep inverted region, where even small changes in the force fields can lead to significant changes in the CT rate constants. Our results demonstrate the importance of combining polarizable force fields with an electronic structure method that can accurately capture the energies of excited CT states when calculating charge-transfer rates.

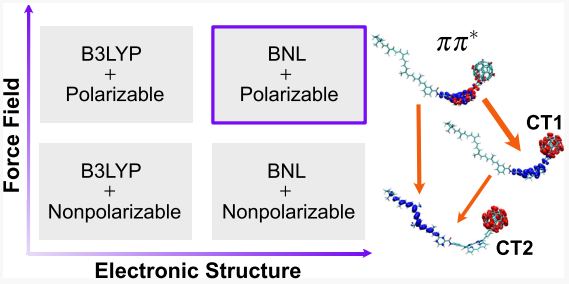

INTRODUCTION

The ability to calculate charge-transfer (CT) rate constants in a complex molecular condensed-phase system accurately and reliably is key for quantitative modeling of many systems with biological and technological importance.[1−5] One reason why modeling CT in such complex systems is challenging is the need to combine multiple methodologies, each of which calls for making choices based on the trade-off between accuracy and computational feasibility.[6] This includes the choice of an electronic structure method,[7] the method used for assigning partial charges,[8] and force fields (e.g., polarizable vs. nonpolarizable).[9]

In this paper, we investigate the effect of the aforementioned choices on the rate constants of the multiple CT processes that occur in the carotenoid−porphyrin−C_{60} (CPC_{60}) molecular triad dissolved in explicit tetrahydrofuran (THF) liquid solvent (see Figure 1a). This system has received much recent attention as a model for understanding photoinduced CT processes similar to those occurring in photosynthetic reaction centers and organic photovoltaic devices.[10−25] In a recent paper, we calculated the rate constants for the various CT processes that occur in this system using nonpolarizable force fields (NFFs) with Mulliken partial charges obtained from time-dependent density functional theory (TDDFT) with the Baer−Neuhauser−Livshits (BNL) density functional.[17] In this paper, we investigate the robustness of the results we obtained in ref 17 by comparing them to results obtained by using polarizable force fields (PFFs),[15,26] using the iterative restrained electrostatic potential method (i-RESP) partial charges based on TDDFT with either BNL or B3LYP functionals. Our main observation is that choosing an electronic structure method that can accurately capture the energies of the excited CT states is key for not only obtaining reliable CT rate constants but also understanding the role of polarizability.

The CT dynamics in the above-mentioned solvated molecular triad system is strongly dependent on the conformation of the triad and is much faster in the linear conformation than in the bent conformation[13,14,16,17] (see the conformations illustrated in Figure 1b). Accounting for this calls for treating the different

Received: July 30, 2020
Published: September 30, 2020

https://dx.doi.org/10.1021/acs.jctc.0c00796
J. Chem. Theory Comput. 2020, 16, 6481−6490

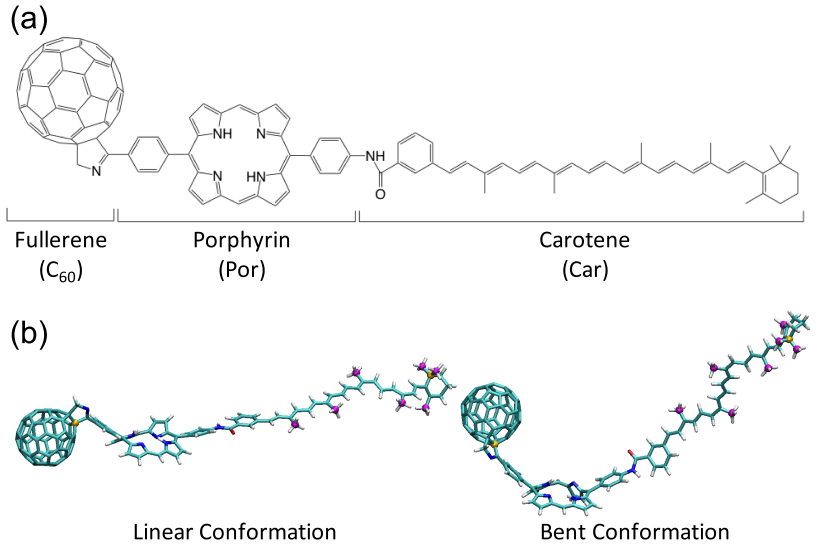

Figure 1. Conformations of the triad molecule showing (a) its three units (fullerene, porphyrin, and carotenoid) and (b) its two structural conformations (linear and bent conformations).

conformations as individual chemical species, each of which associated with a corresponding force field.[13,16] It should also be noted that CT in this system was found to be driven by the solvent degrees of freedom (DOF), rather than by the intramolecular triad DOF.[17] Thus, solvent polarization effects are expected and their effect on the CT dynamics is of interest.

Our model of CPC_{60} takes into account four electronic states of the triad:[14] (1) the ground state, CPC_{60}; (2) the P-localized excitonic $\pi\pi^*$ state, CP^*C_{60}; (3) the excited P-to-C_{60} CT state, $CP^+C_{60}^-$, which is referred to as CT1; and (4) the excited C-to-C_{60} charge-separated state, $C^+PC_{60}^-$, which is referred to as CT2. Following photoexcitation from the ground state to the $\pi\pi^*$ state, the triad is believed to undergo a nonradiative transition from $\pi\pi^*$ to CT1, followed by another nonradiative transition from CT1 to CT2.[14] It should be emphasized that the partial charges are assigned[13,16] for each electronic state (ground, $\pi\pi^*$, CT1, and CT2) at the different conformations (bent and linear) (atomic coordinates and charges are detailed in the Supporting Information (SI)).

COMPUTATIONAL METHODS

Marcus theory rate constants were calculated based on the following expression[17]

$$k_{D\to A}^{M} = \frac{1}{\hbar}\Gamma_{DA}^{2}\sqrt{\frac{2\pi}{\sigma_D^2}}\exp\left[-\frac{\langle U\rangle_D^2}{2\sigma_D^2}\right] \quad (1)$$

Here, Γ_{DA} is the electronic coupling between the donor and acceptor states, $\langle U\rangle_D$ is the average donor−acceptor potential energy gap, $U = V_D(\mathbf{R}, \mathbf{r}) - V_A(\mathbf{R}, \mathbf{r})$, at equilibrium on the donor PES, and $\sigma_D = \sqrt{\langle U^2\rangle_D - \langle U\rangle_D^2}$ is the corresponding standard deviation.[17] $V_D(\mathbf{R}, \mathbf{r})$ and $V_A(\mathbf{R}, \mathbf{r})$ are the PESs of the triad in the donor and in the acceptor states, respectively, and are obtained directly from the MD simulations.[17] The reorganization energy, E_r, and reaction free energy, ΔE, are given by[27−30]

$$E_r = \frac{\sigma_D^2}{2k_B T}$$
$$\Delta E = -E_r - \langle U\rangle_D \quad (2)$$

As illustrated in the algorithm flow chart (Figure 2), the Marcus-like rates are obtained from the triad donor and acceptor

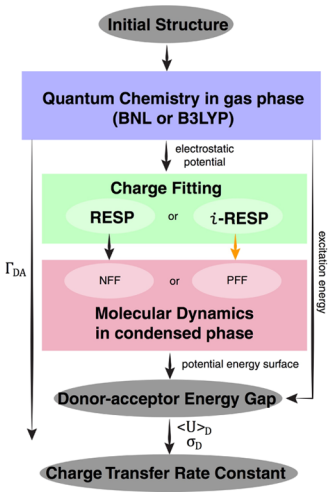

Figure 2. Flow chart of the protocol for obtaining charge-transfer rate constants. The primary steps include gas-phase electronic structure, force field parameterization, and MD simulations to obtain donor and acceptor potential energies. The donor-to-acceptor energy gap parameters and the electronic coupling are used in the rate expression.

potential energy surfaces (V_D and V_A).[6] The starting point for the calculation of the donor−acceptor energy gap is the excitation energies of the triad conformation within the isolated single molecule as obtained via TDDFT, based on B3LYP or BNL. The corresponding electrostatic distributions and atomic partial charges (RESP or i-RESP) are then used to parameterize the force fields (NFF or PFF). Molecular dynamics simulations add the effect of intramolecular and intermolecular nuclear motion that give rise to the V_D and V_A potential energy surfaces. The corresponding energy gap distribution parameters ($\langle U\rangle_D$ and σ_D), along with the electronic coupling coefficients obtained from the gas-phase calculations, are used in the rate expression. Next, we provide further details on the electronic structure and MD calculations.

https://dx.doi.org/10.1021/acs.jctc.0c00796
J. Chem. Theory Comput. 2020, 16, 6481−6490

Table 1. Energy Parameters $\langle U\rangle_D$, σ_D, E_r, ΔE, and Γ_{DA} in eV and Rate Constants in s^{-1} for the Three Electronic Transitions Using the RESP Charges (for the MD Simulations Using NFF) and the i-RESP Charges (for the MD Simulations Using PFF) at the Level of BNL or B3LYP Functionals

			BNL		B3LYP	
			NFF	PFF	NFF	PFF
$\pi\pi^* \rightarrow$ CT1	linear	$\langle U\rangle_D$	−0.329	−0.456	0.977	0.721
		σ_D	0.167	0.221	0.201	0.257
		E_r	0.541	0.954	0.784	1.287
		ΔE	−0.212	−0.498	−1.761	−2.008
		Γ_{DA}	9.0×10^{-3}		5.2×10^{-3}	
		$k^M_{D\rightarrow A}$	2.6×10^{11}	1.7×10^{11}	3.7×10^{6}	7.9×10^{9}
	bent	$\langle U\rangle_D$	0.433	0.194	1.271	1.087
		σ_D	0.159	0.203	0.164	0.212
		E_r	0.494	0.805	0.523	0.875
		ΔE	−0.927	−0.999	−1.795	−1.963
		Γ_{DA}	2.4×10^{-2}		1.8×10^{-2}	
		$k^M_{D\rightarrow A}$	3.4×10^{11}	6.8×10^{12}	6.6×10^{-1}	1.1×10^{7}
$\pi\pi^* \rightarrow$ CT2	linear	$\langle U\rangle_D$	−0.282	−0.868	1.577	1.038
		σ_D	0.281	0.369	0.253	0.339
		E_r	1.539	2.648	1.241	2.232
		ΔE	−1.257	−1.781	−2.819	−3.271
		Γ_{DA}	2.0×10^{-4}		6.4×10^{-6}	
		$k^M_{D\rightarrow A}$	3.3×10^{8}	2.6×10^{7}	2.1×10^{-3}	4.2×10^{3}
	bent	$\langle U\rangle_D$	0.213	−0.470	1.248	0.832
		σ_D	0.260	0.338	0.234	0.310
		E_r	1.320	2.229	1.067	1.876
		ΔE	−1.533	−1.759	−2.316	−2.708
		Γ_{DA}	4.5×10^{-5}		4.3×10^{-6}	
		$k^M_{D\rightarrow A}$	2.1×10^{7}	8.7×10^{6}	2.0×10^{-1}	6.3×10^{3}
CT1 → CT2	linear	$\langle U\rangle_D$	−0.289	−0.853	−0.011	−0.367
		σ_D	0.261	0.366	0.233	0.306
		E_r	1.330	2.611	1.053	1.821
		ΔE	−1.041	−1.759	−1.043	−1.454
		Γ_{DA}	1.0×10^{-3}		2.1×10^{-3}	
		$k^M_{D\rightarrow A}$	7.9×10^{9}	6.9×10^{8}	7.2×10^{10}	2.7×10^{10}
	bent	$\langle U\rangle_D$	−0.793	−1.121	−0.447	−0.812
		σ_D	0.268	0.337	0.228	0.281
		E_r	1.395	2.216	1.009	1.531
		ΔE	−0.602	−1.095	−0.562	−0.719
		Γ_{DA}	8.6×10^{-5}		3.7×10^{-5}	
		$k^M_{D\rightarrow A}$	1.3×10^{6}	3.4×10^{5}	3.3×10^{6}	2.8×10^{5}

Electronic Structure Calculations. Electronic structure calculations of the triad are performed on two representative conformations: (1) the linear conformation of the triad is obtained by geometry optimization in a polarizable continuum model (PCM)[31,32] with switching/Gaussian (SWIG)[33] representing tetrahydrofuran (THF) of a 7.6 scalar dielectric constant employing the B3LYP functional[34,35] with the split-valence (SV) basis set[36,37] for all atoms; and (2) the bent conformation of the triad was selected from the clustered structures of the ensemble of the MD simulations with the explicit THF solvent at 300 K from the previous study.[14]

The excited states are calculated for the single triad at each of the conformations, at the TDDFT[38] level with B3LYP[34,35] and the range-separated hybrid (RSH) BNL functional[39,40] and the same SV basis set level that has been benchmarked successfully by relating to available spectral data.[14] The electronic coupling parameter is obtained via the fragment-charge difference (FCD) method[41] based on the gas-phase TDDFT calculations. The BNL tuning parameter (γ) was calculated using the $J^2(\gamma)$ error minimization tuning scheme[42] in the gas phase. The BNL, as an RSH functional, describes reliably CT states, where the tendency of DFT to underestimate CT state energies is alleviated.[43−46] The electronic properties for the linear as well as the bent conformations at either BNL or B3LYP level are provided in Table S2 in the Supporting Information. All of the electronic structure calculations were performed using the Q-Chem program package.[47]

Conformation-Dependent Force Fields. Our force fields are based on general AMBER force field (GAFF)[48−50] and conformation-dependent sets of partial charges and electronic distribution. Specifically, for PFF, bonded and van der Waals parameters were from GAFF; the polarizabilities were taken from AMBER polarizable force field ff12polL. Details about the development of the partial charges are as follows:

(a) Triad: The atomic partial charges of the relevant excited states in each triad conformation using the two functionals are obtained using two schemes. Charges are obtained by the Mulliken population analysis[51] and the restrained electrostatic potential (RESP) fitting.[52,53] The excited-state electrostatic potentials (ESPs) expressed on

https://dx.doi.org/10.1021/acs.jctc.0c00796
J. Chem. Theory Comput. 2020, 16, 6481−6490

a Lebedev grid point[54] were used in the RESP fitting. We utilized the point dipole method[55] with the Thole-type model (TTM)[56−59] to incorporate the polarization into the force field development. The atomic polarizabilities were taken from the AMBER force field ff12polL as the same in our previous ground-state PFF MD simulation study.[15] Ground-state atomic polarizabilities were used for all electronic states.

(b) THF: The ground-state atomic partial charges of the solvent THF were adopted from our previous study.[15] The ground-state atomic polarizabilities for THF were taken from the AMBER force field ff12polL and are tabulated in the Supporting Information.

Both the Mulliken charges and the RESP charges were used to develop NFFs. For the PFFs, we employed the induced dipole-corrected RESP (i-RESP) charges[26] for the three excited electronic states (i.e., CT1, CT2, $\pi\pi^*$) at both conformations (linear and bent).

Molecular Dynamics Simulations. We obtain the PESs of the triad in the donor and in the acceptor states directly from the MD simulations on the donor state.[17] All MD simulations, with NFF or with PFF, were performed using the AMBER12 program.[60] The pre-equilibrated structures of the triad with 6741 THF molecules in a cubic periodic box (96.9 Å × 96.9 Å × 96.9 Å) were used as an initial condition.[14] Energy minimization was performed using the steepest descent method and the conjugate gradient method, followed by gradually heating to 298.15 K. Constraints were added via a harmonic potential with a force constant of 100 kcal mol^{-1} Å^{-2} (these constraints have a negligible effect in the rate calculations). The SHAKE algorithm[61] was employed for the bond length constraints involving hydrogen atoms. The cutoff distance for non-electrostatic interactions was set to 12 Å, and the particle-mesh Ewald (PME)[62] was used for the long-range electrostatic interactions. The system was equilibrated with NFF at 298.15 K and 1 atmosphere (isothermal−isobaric ensemble, NPT) for 2 ns with the time step of 2 fs to reach the desired density of the system using the Berendsen weak-coupling method[63] and Langevin dynamics[64] for the pressure and temperature control, respectively. For the molecular dynamics simulations with PFF, the same systems equilibrated using NFF were used as initial conditions. The system was re-equilibrated for another 2 ns in a canonical (NVT) ensemble. Following the equilibration, production runs with NFF or PFF were performed for 6 ns in total with the same initial conditions sampled from the previous equilibrated runs. To ensure a smooth distribution of the potential energy gap between the donor and acceptor states, we collected 600,000 frames from each system by sampling at every 10 fs; a similar sampling interval was used in our previous study using NFF.[17] In addition, we show in Table S6 in the Supporting Information that the CT rates based on the first half of the MD trajectories (of 3 ns) are in good agreement, within an order of magnitude, with the rates based on the full 6 ns MD trajectories.

In total, we performed MD simulations on the donor states for each of the three CT processes ($\pi\pi^* \rightarrow$ CT1, $\pi\pi^* \rightarrow$ CT2, and CT1 → CT2). The potential energy on the acceptor states was calculated from the donor-state MD trajectories. Afterward, the energy gap U was corrected by the QM excitation energy following eq 13 in ref 17.

RESULTS AND DISCUSSION

The rate constants for the three electronic transitions obtained by using the RESP charges (when the MD simulations are based on NFF) and the i-RESP charges (when the MD simulations are based on PFF), and the BNL or B3LYP functionals, are shown in Table 1. Also shown in this table are the corresponding values of $\langle U \rangle_D$, σ_D, E_r, ΔE, and Γ_{DA} that determine the rate constants. (Mulliken-charge-based energies are provided for reference in Table S1.)

A close inspection of the results reveals that BNL generally leads to better estimation of the CT rate constants. The rate constants obtained using B3LYP for the $\pi\pi^* \rightarrow$ CT1 and $\pi\pi^* \rightarrow$ CT2 transitions are orders of magnitude smaller than the rate constants obtained for those transitions using BNL. This difference can be traced back to the fact that B3LYP overstabilizes the CT1 and CT2 states relative to the $\pi\pi^*$ state[65−67] and thereby leads to greater negative values of ΔE relative to BNL. As a result, the $\pi\pi^* \rightarrow$ CT1 and $\pi\pi^* \rightarrow$ CT2 transitions are shifted deeper into the inverted region when B3LYP is used, where the rate constants are significantly smaller compared to their values in the close vicinity of the Marcus turnover region. In contrast, when BNL is used, the $\pi\pi^* \rightarrow$ CT1 and $\pi\pi^* \rightarrow$ CT2 transitions are in either the normal or shallow inverted region and thereby significantly faster. See these energy trends where B3LYP overstabilizes the CT state in comparison to BNL illustrated for the $\pi\pi^* \rightarrow$ CT transitions at the linear conformation in Figure 3 with the energies listed in Table 2. It should be noted that the BNL-based rate constants are

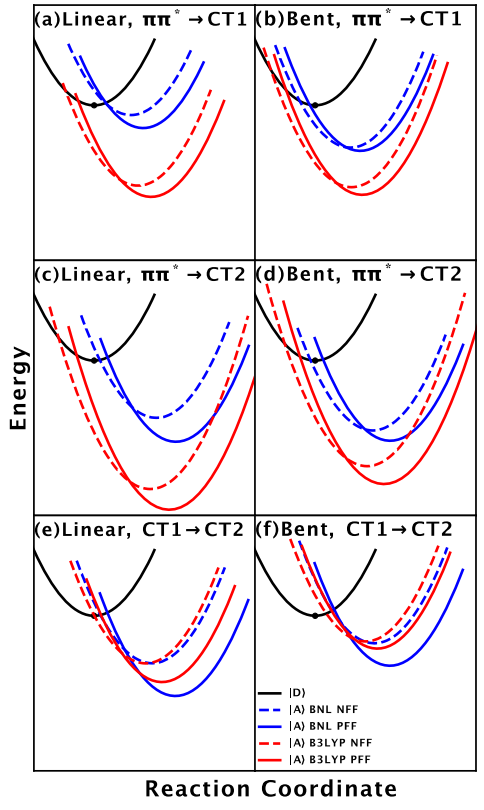

Figure 3. Parabolic potential energy surfaces comparing BNL (blue) and B3LYP (red) for the different transitions at the linear and bent conformations. B3LYP finds larger stabilization of the CT state over the $\pi\pi^*$ state than that indicated by BNL. This trend is even reversed for the CT1 → CT2 transition due to cancellation of errors in the B3LYP case.

https://dx.doi.org/10.1021/acs.jctc.0c00796
J. Chem. Theory Comput. 2020, 16, 6481−6490

Table 2. Charge-Transfer Rate Constants in s^{-1} from a Donor to an Acceptor Electron State ($k^{M}_{D\to A}$) Calculated from the MD Simulations with the Mulliken Charges and with the RESP Charges (for the MD Simulations Using NFF) and the i-RESP Charges (for the MD Simulations Using PFF) at the Level of BNL or B3LYP[a]

		BNL		B3LYP	
		NFF	PFF	NFF	PFF
$\pi\pi^*$ → CT1	linear-Mulliken	1.2×10^{12}	5.5×10^{11}	7.8×10^{6}	1.0×10^{10}
	linear-RESP/i-RESP	2.6×10^{11}	1.7×10^{11}	3.7×10^{6}	7.9×10^{9}
	bent-Mulliken	2.8×10^{10}	5.1×10^{12}	1.1×10^{2}	2.3×10^{9}
	bent-RESP/i-RESP	3.4×10^{11}	6.8×10^{12}	6.6×10^{-1}	1.1×10^{7}
$\pi\pi^*$ → CT2	linear-Mulliken	3.9×10^{8}	8.4×10^{7}	5.2×10^{-2}	4.0×10^{3}
	linear-RESP/i-RESP	3.3×10^{8}	2.6×10^{7}	2.1×10^{-3}	4.2×10^{3}
	bent-Mulliken	1.9×10^{7}	1.9×10^{7}	3.5	2.4×10^{4}
	bent-RESP/i-RESP	2.1×10^{7}	8.7×10^{6}	2.0×10^{-1}	6.3×10^{3}
CT1 → CT2	linear-Mulliken	3.7×10^{9}	1.2×10^{9}	7.0×10^{8}	5.5×10^{9}
	linear-RESP/i-RESP	7.9×10^{9}	6.9×10^{8}	7.2×10^{10}	2.7×10^{10}
	bent-Mulliken	8.3×10^{4}	4.1×10^{5}	5.8×10^{2}	8.4×10^{4}
	bent-RESP/i-RESP	1.3×10^{6}	3.4×10^{5}	3.3×10^{6}	2.8×10^{5}

[a]The measured CT rates[23] are as follows: $k(\pi\pi^* \to \mathrm{CT1}) = 3.3 \times 10^{11}\ s^{-1}$ and $k(\mathrm{CT1} \to \mathrm{CT2}) = 1.5 \times 10^{10}\ s^{-1}$.

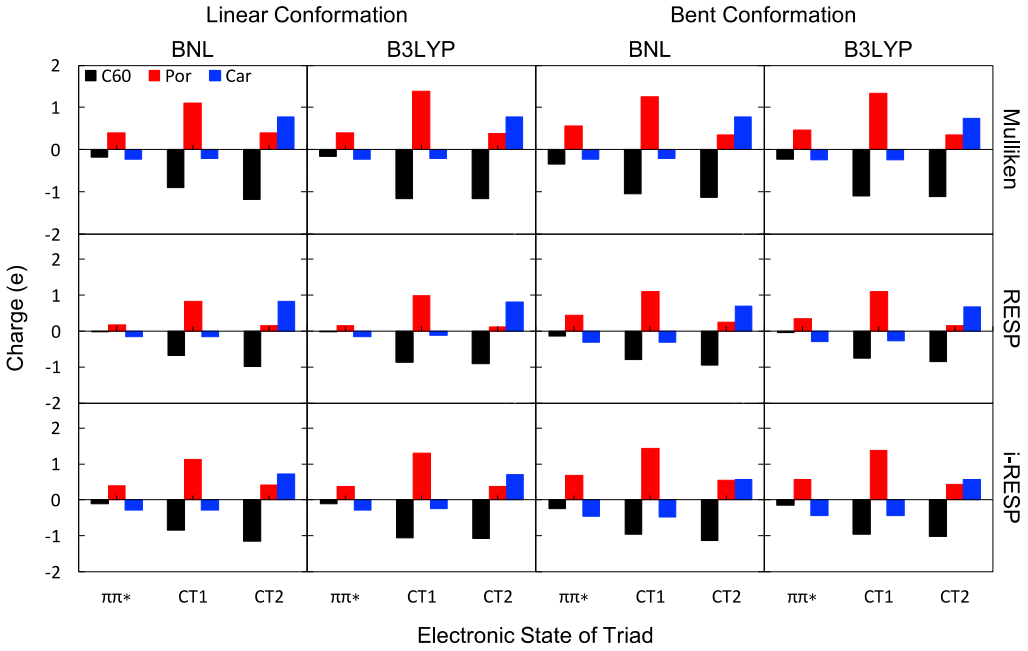

Figure 4. Net charges from the $\pi\pi^*$, the CT1, and the CT2 states on the three subunits: C_{60} (black), porphyrin (red), and carotenoid (blue) in both linear and bent conformations using the Mulliken (top), RESP (middle), and i-RESP (bottom) charge models obtained at the level of BNL or B3LYP functionals, respectively. See Table S3 in the SI for the numerical values.

consistent with the corresponding experimental values (Table 2), which suggests that BNL yields a more accurate electronic structure. This is consistent with the well-documented ability of BNL to give accurate energies for CT states and the inability of B3LYP to do so.[42−44,68]

The rate constant obtained using B3LYP for the CT1 → CT2 transition is similar to the rate constants obtained for this transition using BNL. This is because in this case, the values of ΔE obtained from BNL and B3LYP are similar. Thus, even though B3LYP overstabilizes the energies of the CT1 and CT2 states, the overstabilization effect mostly cancels out since ΔE corresponds to the difference in the energies of those two states. Similar observations are found when Mulliken charges are used (Table S1). Therefore, the choice of the method used for assigning partial charges appears to have only a minor effect on the CT rate constants.

Another noteworthy observation is that PFF can compensate for the overstabilization of CT states by B3LYP. More specifically, changing from NFF to PFF is generally seen to increase E_r by a factor of 1.5−2.0 for both B3LYP and BNL. This can be traced back to the fact that accounting for polarization effects further stabilizes upon solvation. Changing from NFF to PFF is also seen to lead to more negative values of ΔE. This can be traced back to the fact that accounting for polarization effects adds extra stabilization to the CT1 and CT2 states relative to the $\pi\pi^*$ state as well as to the CT2 state relative to the CT1 state due to the larger dipole moment of the former (see Tables S4 and S5, and Figure S1 in the Supporting Information). However, changing from NFF to PFF has a rather modest effect on the rate constants for the $\pi\pi^*$ → CT1 and $\pi\pi^*$ → CT2 transitions when calculated using BNL, which are observed to change by no more than 1 order of magnitude due to it. In contrast, changing from

https://dx.doi.org/10.1021/acs.jctc.0c00796
J. Chem. Theory Comput. 2020, 16, 6481−6490

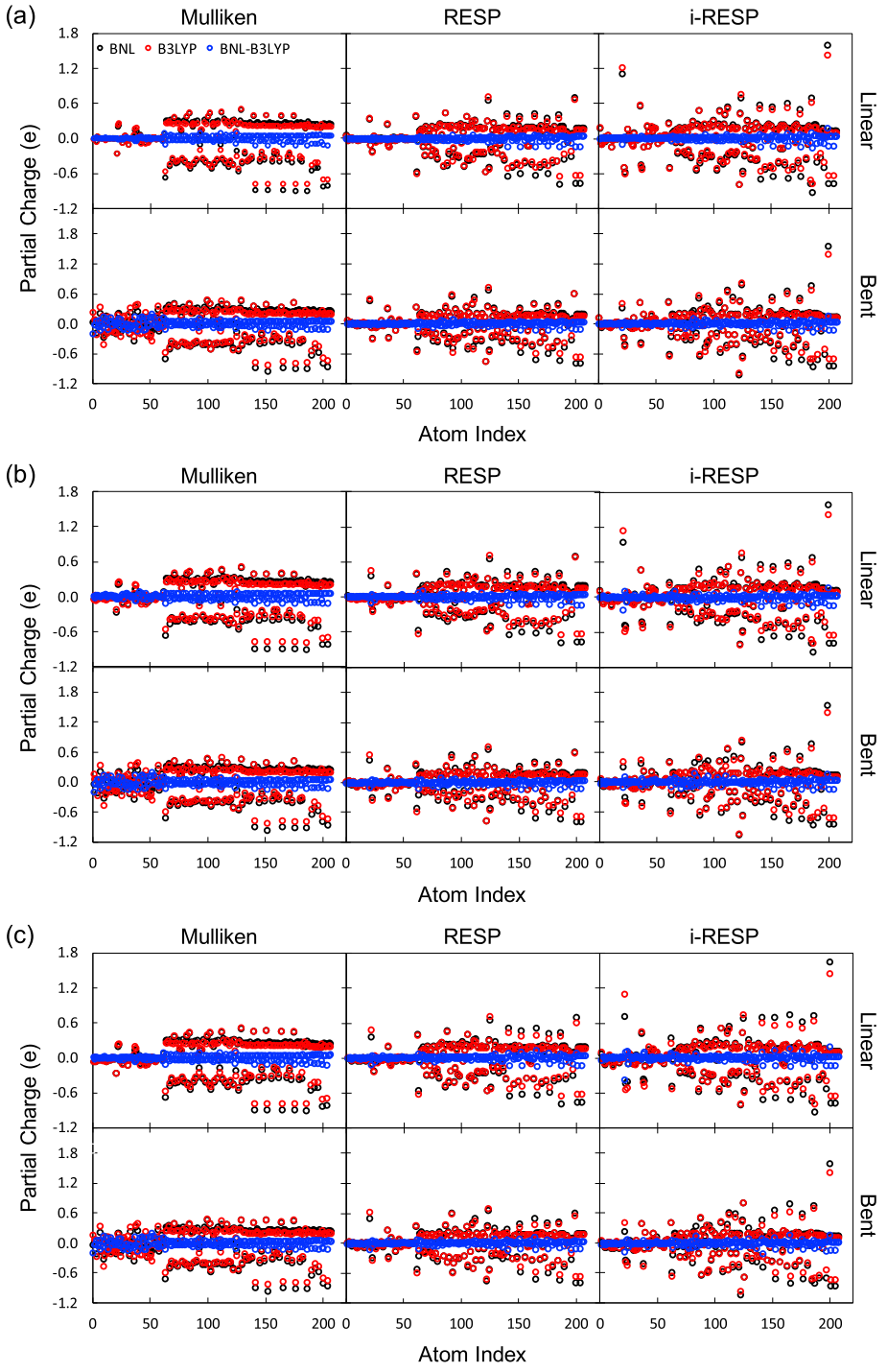

Figure 5. Atomic partial charges of the triad in (a) the $\pi\pi^*$, (b) the CT1, and (c) the CT2 states. In each panel, the top row is for the linear and the bottom row is for the bent conformations. In each panel, the left column is from the Mulliken charge model, the middle column is from the RESP charge model, and the right column is from the i-RESP charge models. The charges obtained at the BNL level are in black circles, those obtained at the B3LYP level are in red circles, and the differences in the partial charges between the two ($\Delta q = q_{BNL} - q_{B3LYP}$) are in blue circles. See the detailed atomic charges in the SI.

NFF to PFF has a dramatic effect on the rate constants for the $\pi\pi^* \rightarrow$ CT1 and $\pi\pi^* \rightarrow$ CT2 transitions when B3LYP is used, changing them by 3−8 orders of magnitude.

This behavior of increased sensitivity to use PFF by B3LYP can be traced back to the above-mentioned tendency of B3LYP to push the transition to the deep inverted region when relatively modest changes in ΔE and E_r give rise to large changes in the rate constant. In contrast, the same transitions are in the close vicinity of the Marcus turnover region when BNL is used, either in the normal or in the shallow inverted region, where modest changes in ΔE and E_r give rise to similarly modest changes in the rate constant. Thus, changing from NFF to PFF increases the rate constants obtained by using B3LYP and brings them much closer to the rate constants obtained by using BNL with either NFF or PFF. Hence, using B3LYP may give the impression that polarization bears a significant impact on the rate and that

https://dx.doi.org/10.1021/acs.jctc.0c00796
J. Chem. Theory Comput. 2020, 16, 6481−6490

accounting for it is necessary for obtaining accurate rate constants. However, this dramatic effect on the rate constants of adding polarization effects appears to be fortuitous, rather than due to the actual underlying physics. Indeed, by using a more reliable functional when it comes to predicting the energies of CT states like BNL already yields pretty accurate results with the NFF.

Finally, we consider the sensitivity of the rate constants to the choice of method for assigning atomic charges (see Figures 4 and 5, and Table 2). The results show that BNL and B3LYP give rise to rather similar CT rates, regardless of which method is used to assign them (Mulliken or RESP/i-RESP). As a result, the CT rate constants are seen to be relatively insensitive to whether Mulliken or RESP/i-RESP is used to assign atomic charges (see Table 2).

CONCLUDING REMARKS

In this paper, we considered the interplay between the choice of an electronic structure method and the effect of using polarizable force fields vs. nonpolarizable force fields when calculating solution-phase CT rates in the CPC_{60} molecular triad dissolved in the explicit THF liquid solvent. To this end, we compared Marcus theory rate constants that were calculated for this system based on classical MD simulations using PFF and NFF obtained via TDDFT with the BNL and B3LYP functionals.

Our main conclusion is that the most important factor determining the accuracy of the CT rate constants is the choice of an electronic structure method. The rate constants obtained using BNL were observed to be in much better agreement with the available experimental values than those obtained via B3LYP. This behavior can be traced back to the well-documented tendency of B3LYP to overstabilize the energies of CT states, which was observed to push the system into the far-inverted regime and thereby significantly slow down CT rates.

Our results also underscore the importance of combining the use of PFF with an electronic structure method that quantitatively captures the energies of the excited CT states and not just the corresponding atomic charges. As we have shown, failing to do so can lead to the erroneous conclusion that accounting for polarization effects can have a dramatic effect on the CT rates, whereas in reality, those effects are much smaller. Furthermore, electronic-state-dependent polarizability models could be important in the CT rate calculation[69] and will be reported in future publications. Furthermore, embedded TDDFT-based calculations addressing the distribution of the optical response due to the environment will also be reported in future publications.

ASSOCIATED CONTENT

Supporting Information

The Supporting Information is available free of charge at https://pubs.acs.org/doi/10.1021/acs.jctc.0c00796.

Dipole moments of the triad in the excited states (Text S1); excitation-state energies for absorbing (E_{abs}), CT states (E_{CT}), charge separation (ΔQ), and FCD electronic coupling (Γ) of triad (Table S1); calculated $\langle U\rangle_D$, σ_D, E_r, and ΔE for CT reactions of triad with Mulliken charges in the unit of eV (Table S2); net charges on the three subunits of triad in the $\pi\pi^*$, CT1, and CT2 states in the linear and the bent conformations from Mulliken, RESP, and i-RESP charge models obtained at BNL and B3LYP functionals in the unit of e (Table S3); magnitudes of the average dipole moments of triad from MD simulations with Mulliken charges in the unit of Debye (Table S4); list of magnitudes of the average dipole moments of triad from MD simulations with RESP (NFF) and i-RESP (PFF) charges in the unit of Debye (Table S5); energy parameters $\langle U\rangle_D$, σ_D, E_r, ΔE, and Γ_{DA} and rate constants for the three electronic transitions using the RESP/i-RESP charges (for the MD simulations using NFF/PFF, respectively) at the level of BNL or B3LYP functionals; first halves of frames in the MD trajectories (3 ns) were used (Table S6); and comparison of dipole moments from the PFF MD simulations with (a) Mulliken charges and (b) i-RESP charges from BNL and B3LYP functionals in excited states (Figure S1) (PDF)

XYZ coordinates, atom names, ground-state atomic polarizabilities, and atomic charges of the triad/THF (XLSX)

AUTHOR INFORMATION

Corresponding Authors

Xiang Sun − *Division of Arts and Sciences and NYU-ECNU Center for Computational Chemistry, NYU Shanghai, Shanghai 200122, China; Department of Chemistry, New York University, New York, New York 10003, United States;* orcid.org/0000-0002-2846-8532; Email: xiang.sun@nyu.edu

Eitan Geva − *Department of Chemistry, University of Michigan, Ann Arbor, Michigan 48109, United States;* orcid.org/0000-0002-7935-4586; Email: eitan@umich.edu

Barry D. Dunietz − *Department of Chemistry, Kent State University, Kent, Ohio 44242, United States;* orcid.org/0000-0002-6982-8995; Email: bdunietz@kent.edu

Margaret S. Cheung − *Department of Physics, University of Houston, Houston, Texas 77204, United States; Center for Theoretical Biological Physics, Rice University, Houston, Texas 77005, United States;* orcid.org/0000-0001-9235-7661; Email: mscheung@uh.edu

Authors

Jaebeom Han − *Department of Physics, University of Houston, Houston, Texas 77204, United States;* orcid.org/0000-0001-5709-2389

Pengzhi Zhang − *Department of Physics, University of Houston, Houston, Texas 77204, United States*

Huseyin Aksu − *Department of Chemistry, Kent State University, Kent, Ohio 44242, United States; Department of Physics, Canakkale Onsekiz Mart University, Çanakkale 17100, Turkey;* orcid.org/0000-0001-9463-3236

Buddhadev Maiti − *Department of Chemistry, Kent State University, Kent, Ohio 44242, United States*

Complete contact information is available at: https://pubs.acs.org/10.1021/acs.jctc.0c00796

Author Contributions

J.H., P.Z., H.A., and B.M. ran the simulations and analyzed the data; and X.S., E.G., B.D.D., and M.S.C designed the research and analysis and wrote the paper.

Notes

The authors declare no competing financial interest.

ACKNOWLEDGMENTS

We thank Zengkui Liu for making Figure 3. E.G., B.D.D., and M.S.C. acknowledge the support from the Department of

Energy (DOE) Basic Energy Sciences through the Chemical Sciences, Geosciences, and Biosciences Division (No. DE-SC0016501). X.S. acknowledges the support from the National Natural Science Foundation of China (No. 21903054). J. H. acknowledges computational resources provided by the National Energy Research Scientific Computing Center (NERSC) and by the Research Computing Data Core at the University of Houston. B.D.D. acknowledges computational resources provided by the Ohio Supercomputer Center[70] and the Kent State University, College of Arts and Sciences Computing Cluster.

REFERENCES

(1) Barbara, P. F.; Meyer, T. J.; Ratner, M. A. Contemporary Issues in Electron Transfer Research. *J. Phys. Chem. A* **1996**, *100*, 13148−13168.
(2) Chandler, D. Electron Transfer in Water and Other Polar Environments, How it Happens. In *Classical and Quantum Dynamics in Condensed Phase Simulations*; World Scientific, 1998; pp 25−49.
(3) Weiss, U. *Quantum Dissipative Systems*; World Scientific, 2011.
(4) Kornyshev, A. Chemical Dynamics in Condensed Phases. Relaxation, Transfer and Reactions in Condensed Matter Molecular Systems. By Abraham Nitzan. *ChemPhysChem* **2007**, *8*, 1250−1252.
(5) May, V.; Kühn, O. *Charge and Energy Transfer Dynamics in Molecular Systems*; John Wiley & Sons, 2008.
(6) Tinnin, J.; Bhandari, S.; Zhang, P.; Aksu, H.; Maiti, B.; Geva, E.; Dunietz, B. D.; Sun, X.; Cheung, M. S. Molecular-Level Exploration of the Structure-Function Relations Underlying Interfacial Charge Transfer in the Subphthalocyanine/C60 Organic Photovoltaic System. *Phys. Rev. Appl.* **2020**, *13*, No. 054075.
(7) Cohen, A. J.; Mori-Sanchez, P.; Yang, W. Challenges for density functional theory. *Chem. Rev.* **2012**, *112*, 289−320.
(8) Li, P.; Merz, K. M., Jr. Metal Ion Modeling Using Classical Mechanics. *Chem. Rev.* **2017**, *117*, 1564−1686.
(9) Leontyev, I.; Stuchebrukhov, A. Accounting for electronic polarization in non-polarizable force fields. *Phys. Chem. Chem. Phys.* **2011**, *13*, 2613−2626.
(10) Liu, J.; Zhang, Y.; Liu, W. Photoexcitation of Light-Harvesting C-P-C60 Triads: A FLMO-TD-DFT Study. *J. Chem. Theory Comput.* **2014**, *10*, 2436−2448.
(11) Olguin, M.; Basurto, L.; Zope, R. R.; Baruah, T. The effect of structural changes on charge transfer states in a light-harvesting carotenoid-diaryl-porphyrin-C60 molecular triad. *J. Chem. Phys.* **2014**, *140*, No. 204309.
(12) Patel, K.; Bittner, E. R. Mixed Quantum Classical Simulations of Charge-Transfer Dynamics in a Model Light-Harvesting Complex. I. Charge-Transfer Dynamics. *J. Phys. Chem. B* **2020**, *124*, 2149−2157.
(13) Balamurugan, D.; Aquino, A. J.; de Dios, F.; Flores, L., Jr.; Lischka, H.; Cheung, M. S. Multiscale simulation of the ground and photo-induced charge-separated states of a molecular triad in polar organic solvent: exploring the conformations, fluctuations, and free energy landscapes. *J. Phys. Chem. B* **2013**, *117*, 12065−12075.
(14) Manna, A. K.; Balamurugan, D.; Cheung, M. S.; Dunietz, B. D. Unraveling the Mechanism of Photoinduced Charge Transfer in Carotenoid-Porphyrin-C60 Molecular Triad. *J. Phys. Chem. Lett.* **2015**, *6*, 1231−1237.
(15) Starovoytov, O. N.; Zhang, P.; Cieplak, P.; Cheung, M. S. Induced polarization restricts the conformational distribution of a light-harvesting molecular triad in the ground state. *Phys. Chem. Chem. Phys.* **2017**, *19*, 22969−22980.
(16) Su, G.; Czader, A.; Homouz, D.; Bernardes, G.; Mateen, S.; Cheung, M. S. Multiscale simulation on a light-harvesting molecular triad. *J. Phys. Chem. B* **2012**, *116*, 8460−8473.
(17) Sun, X.; Zhang, P.; Lai, Y.; Williams, K. L.; Cheung, M. S.; Dunietz, B. D.; Geva, E. Computational Study of Charge-Transfer Dynamics in the Carotenoid−Porphyrin−C60Molecular Triad Solvated in Explicit Tetrahydrofuran and Its Spectroscopic Signature. *J. Phys. Chem. C* **2018**, *122*, 11288−11299.
(18) Rego, L. G. C.; Hames, B. C.; Mazon, K. T.; Joswig, J.-O. Intramolecular Polarization Induces Electron−Hole Charge Separation in Light-Harvesting Molecular Triads. *J. Phys. Chem. C* **2014**, *118*, 126−134.
(19) Gust, D.; Moore, T. A.; Moore, A. L. Mimicking photosynthetic solar energy transduction. *Acc. Chem. Res.* **2001**, *34*, 40−48.
(20) Kodis, G.; Liddell, P. A.; Moore, A. L.; Moore, T. A.; Gust, D. Synthesis and photochemistry of a carotene−porphyrin−fullerene model photosynthetic reaction center. *J. Phys. Org. Chem.* **2004**, *17*, 724−734.
(21) Kuciauskas, D.; Liddell, P. A.; Lin, S.; Stone, S. G.; Moore, A. L.; Moore, T. A.; Gust, D. Photoinduced Electron Transfer in Carotenoporphyrin−Fullerene Triads: Temperature and Solvent Effects. *J. Phys. Chem. B* **2000**, *104*, 4307−4321.
(22) Liddell, P. A.; Kuciauskas, D.; Sumida, J. P.; Nash, B.; Nguyen, D.; Moore, A. L.; Moore, T. A.; Gust, D. Photoinduced Charge Separation and Charge Recombination to a Triplet State in a Carotene−Porphyrin−Fullerene Triad. *J. Am. Chem. Soc.* **1997**, *119*, 1400−1405.
(23) Smirnov, S. N.; Liddell, P. A.; Vlassiouk, I. V.; Teslja, A.; Kuciauskas, D.; Braun, C. L.; Moore, A. L.; Moore, T. A.; Gust, D. Characterization of the Giant Transient Dipole Generated by Photoinduced Electron Transfer in a Carotene−Porphyrin−Fullerene Molecular Triad. *J. Phys. Chem. A* **2003**, *107*, 7567−7573.
(24) Baruah, T.; Pederson, M. R. Density functional study on a light-harvesting carotenoid-porphyrin-C[sub 60] molecular triad. *J. Chem. Phys.* **2006**, *125*, No. 164706.
(25) Baruah, T.; Pederson, M. R. DFT Calculations on Charge-Transfer States of a Carotenoid-Porphyrin-C60 Molecular Triad. *J. Chem. Theory Comput.* **2009**, *5*, 834−843.
(26) Cieplak, P.; Caldwell, J.; Kollman, P. Molecular mechanical models for organic and biological systems going beyond the atom centered two body additive approximation: aqueous solution free energies of methanol and N-methyl acetamide, nucleic acid base, and amide hydrogen bonding and chloroform/water partition coefficients of the nucleic acid bases. *J. Comput. Chem.* **2001**, *22*, 1048−1057.
(27) Sun, X.; Geva, E. Equilibrium Fermi's Golden Rule Charge Transfer Rate Constants in the Condensed Phase: The Linearized Semiclassical Method vs Classical Marcus Theory. *J. Phys. Chem. A* **2016**, *120*, 2976−2990.
(28) Schulten, K.; Tesch, M. Coupling of protein motion to electron transfer: Molecular dynamics and stochastic quantum mechanics study of photosynthetic reaction centers. *Chem. Phys.* **1991**, *158*, 421−446.
(29) Muegge, I.; Qi, P. X.; Wand, A. J.; Chu, Z. T.; Warshel, A. The Reorganization Energy of CytochromecRevisited. *J. Phys. Chem. B* **1997**, *101*, 825−836.
(30) King, G.; Warshel, A. Investigation of the free energy functions for electron transfer reactions. *J. Chem. Phys.* **1990**, *93*, 8682−8692.
(31) Tomasi, J.; Mennucci, B.; Cammi, R. Quantum mechanical continuum solvation models. *Chem. Rev.* **2005**, *105*, 2999−3093.
(32) Mewes, J. M.; You, Z. Q.; Wormit, M.; Kriesche, T.; Herbert, J. M.; Dreuw, A. Experimental benchmark data and systematic evaluation of two a posteriori, polarizable-continuum corrections for vertical excitation energies in solution. *J. Phys. Chem. A* **2015**, *119*, 5446−5464.
(33) Lange, A. W.; Herbert, J. M. Polarizable Continuum Reaction-Field Solvation Models Affording Smooth Potential Energy Surfaces. *J. Phys. Chem. Lett.* **2010**, *1*, 556−561.
(34) Becke, A. D. Density-functional thermochemistry. III. The role of exact exchange. *J. Chem. Phys.* **1993**, *98*, 5648−5652.
(35) Lee, C.; Yang, W.; Parr, R. G. Development of the Colle-Salvetti correlation-energy formula into a functional of the electron density. *Phys. Rev. B* **1988**, *37*, 785−789.
(36) Weigend, F.; Ahlrichs, R. Balanced basis sets of split valence, triple zeta valence and quadruple zeta valence quality for H to Rn: Design and assessment of accuracy. *Phys. Chem. Chem. Phys.* **2005**, *7*, 3297−3305.
(37) Schäfer, A.; Horn, H.; Ahlrichs, R. Fully optimized contracted Gaussian basis sets for atoms Li to Kr. *J. Chem. Phys.* **1992**, *97*, 2571−2577.

https://dx.doi.org/10.1021/acs.jctc.0c00796
J. Chem. Theory Comput. 2020, 16, 6481−6490

(38) Runge, E.; Gross, E. K. U. Density-Functional Theory for Time-Dependent Systems. *Phys. Rev. Lett.* **1984**, *52*, 997−1000.
(39) Baer, R.; Neuhauser, D. Density functional theory with correct long-range asymptotic behavior. *Phys. Rev. Lett.* **2005**, *94*, No. 043002.
(40) Livshits, E.; Baer, R. A well-tempered density functional theory of electrons in molecules. *Phys. Chem. Chem. Phys.* **2007**, *9*, 2932−2941.
(41) Voityuk, A. A.; Rösch, N. Fragment charge difference method for estimating donor−acceptor electronic coupling: Application to DNA π-stacks. *J. Chem. Phys.* **2002**, *117*, 5607−5616.
(42) Kuritz, N.; Stein, T.; Baer, R.; Kronik, L. Charge-Transfer-Like pi−>pi* Excitations in Time-Dependent Density Functional Theory: A Conundrum and Its Solution. *J. Chem. Theory Comput.* **2011**, *7*, 2408−2415.
(43) Zheng, S.; Phillips, H.; Geva, E.; Dunietz, B. D. Ab initio study of the emissive charge-transfer states of solvated chromophore-functionalized silsesquioxanes. *J. Am. Chem. Soc.* **2012**, *134*, 6944−6947.
(44) Bhandari, S.; Dunietz, B. D. Quantitative Accuracy in Calculating Charge Transfer State Energies in Solvated Molecular Complexes Using a Screened Range Separated Hybrid Functional within a Polarized Continuum Model. *J. Chem. Theory Comput.* **2019**, *15*, 4305−4311.
(45) Kronik, L.; Stein, T.; Refaely-Abramson, S.; Baer, R. Excitation Gaps of Finite-Sized Systems from Optimally Tuned Range-Separated Hybrid Functionals. *J. Chem. Theory Comput.* **2012**, *8*, 1515−1531.
(46) Stein, T.; Kronik, L.; Baer, R. Prediction of charge-transfer excitations in coumarin-based dyes using a range-separated functional tuned from first principles. *J. Chem. Phys.* **2009**, *131*, No. 244119.
(47) Shao, Y.; Gan, Z.; Epifanovsky, E.; Gilbert, A. T. B.; Wormit, M.; Kussmann, J.; Lange, A. W.; Behn, A.; Deng, J.; Feng, X.; Ghosh, D.; Goldey, M.; Horn, P. R.; Jacobson, L. D.; Kaliman, I.; Khaliullin, R. Z.; Kuś, T.; Landau, A.; Liu, J.; Proynov, E. I.; Rhee, Y. M.; Richard, R. M.; Rohrdanz, M. A.; Steele, R. P.; Sundstrom, E. J.; Woodcock, H. L.; Zimmerman, P. M.; Zuev, D.; Albrecht, B.; Alguire, E.; Austin, B.; Beran, G. J. O.; Bernard, Y. A.; Berquist, E.; Brandhorst, K.; Bravaya, K. B.; Brown, S. T.; Casanova, D.; Chang, C.-M.; Chen, Y.; Chien, S. H.; Closser, K. D.; Crittenden, D. L.; Diedenhofen, M.; DiStasio, R. A.; Do, H.; Dutoi, A. D.; Edgar, R. G.; Fatehi, S.; Fusti-Molnar, L.; Ghysels, A.; Golubeva-Zadorozhnaya, A.; Gomes, J.; Hanson-Heine, M. W. D.; Harbach, P. H. P.; Hauser, A. W.; Hohenstein, E. G.; Holden, Z. C.; Jagau, T.-C.; Ji, H.; Kaduk, B.; Khistyaev, K.; Kim, J.; Kim, J.; King, R. A.; Klunzinger, P.; Kosenkov, D.; Kowalczyk, T.; Krauter, C. M.; Lao, K. U.; Laurent, A. D.; Lawler, K. V.; Levchenko, S. V.; Lin, C. Y.; Liu, F.; Livshits, E.; Lochan, R. C.; Luenser, A.; Manohar, P.; Manzer, S. F.; Mao, S.-P.; Mardirossian, N.; Marenich, A. V.; Maurer, S. A.; Mayhall, N. J.; Neuscamman, E.; Oana, C. M.; Olivares-Amaya, R.; O'Neill, D. P.; Parkhill, J. A.; Perrine, T. M.; Peverati, R.; Prociuk, A.; Rehn, D. R.; Rosta, E.; Russ, N. J.; Sharada, S. M.; Sharma, S.; Small, D. W.; Sodt, A.; Stein, T.; Stück, D.; Su, Y.-C.; Thom, A. J. W.; Tsuchimochi, T.; Vanovschi, V.; Vogt, L.; Vydrov, O.; Wang, T.; Watson, M. A.; Wenzel, J.; White, A.; Williams, C. F.; Yang, J.; Yeganeh, S.; Yost, S. R.; You, Z.-Q.; Zhang, I. Y.; Zhang, X.; Zhao, Y.; Brooks, B. R.; Chan, G. K. L.; Chipman, D. M.; Cramer, C. J.; Goddard, W. A.; Gordon, M. S.; Hehre, W. J.; Klamt, A.; Schaefer, H. F.; Schmidt, M. W.; Sherrill, C. D.; Truhlar, D. G.; Warshel, A.; Xu, X.; Aspuru-Guzik, A.; Baer, R.; Bell, A. T.; Besley, N. A.; Chai, J.-D.; Dreuw, A.; Dunietz, B. D.; Furlani, T. R.; Gwaltney, S. R.; Hsu, C.-P.; Jung, Y.; Kong, J.; Lambrecht, D. S.; Liang, W.; Ochsenfeld, C.; Rassolov, V. A.; Slipchenko, L. V.; Subotnik, J. E.; Van Voorhis, T.; Herbert, J. M.; Krylov, A. I.; Gill, P. M. W.; Head-Gordon, M. Advances in molecular quantum chemistry contained in the Q-Chem 4 program package. *Mol. Phys.* **2015**, *113*, 184−215.
(48) Cornell, W. D.; Cieplak, P.; Bayly, C. I.; Gould, I. R.; Merz, K. M.; Ferguson, D. M.; Spellmeyer, D. C.; Fox, T.; Caldwell, J. W.; Kollman, P. A. A Second Generation Force Field for the Simulation of Proteins, Nucleic Acids, and Organic Molecules. *J. Am. Chem. Soc.* **1995**, *117*, 5179−5197.
(49) Cornell, W. D.; Cieplak, P.; Bayly, C. I.; Gould, I. R.; Merz, K. M.; Ferguson, D. M.; Spellmeyer, D. C.; Fox, T.; Caldwell, J. W.; Kollman, P. A. A Second Generation Force Field for the Simulation of Proteins, Nucleic Acids, and Organic MoleculesJ.Am.Chem.Soc.1995,117, 5179−5197. *J. Am. Chem. Soc.* **1996**, *118*, 2309.
(50) Wang, J.; Wolf, R. M.; Caldwell, J. W.; Kollman, P. A.; Case, D. A. Development and testing of a general amber force field. *J. Comput. Chem.* **2004**, *25*, 1157−1174.
(51) Mulliken, R. S. Electronic Population Analysis on LCAO−MO Molecular Wave Functions. I. *J. Chem. Phys.* **1955**, *23*, 1833−1840.
(52) Bayly, C. I.; Cieplak, P.; Cornell, W.; Kollman, P. A. A well-behaved electrostatic potential based method using charge restraints for deriving atomic charges: the RESP model. *J. Phys. Chem. B* **1993**, *97*, 10269−10280.
(53) Cieplak, P.; Cornell, W. D.; Bayly, C.; Kollman, P. A. Application of the multimolecule and multiconformational RESP methodology to biopolymers: Charge derivation for DNA, RNA, and proteins. *J. Comput. Chem.* **1995**, *16*, 1357−1377.
(54) Singh, U. C.; Kollman, P. A. A combinedab initio quantum mechanical and molecular mechanical method for carrying out simulations on complex molecular systems: Applications to the CH3Cl + Cl? exchange reaction and gas phase protonation of polyethers. *J. Comput. Chem.* **1986**, *7*, 718−730.
(55) Applequist, J.; Carl, J. R.; Fung, K.-K. Atom dipole interaction model for molecular polarizability. Application to polyatomic molecules and determination of atom polarizabilities. *J. Am. Chem. Soc.* **1972**, *94*, 2952−2960.
(56) Thole, B. T. Molecular polarizabilities calculated with a modified dipole interaction. *Chem. Phys.* **1981**, *59*, 341−350.
(57) van Duijnen, P. T.; Swart, M. Molecular and Atomic Polarizabilities: Thole's Model Revisited. *J. Phys. Chem. A* **1998**, *102*, 2399−2407.
(58) Simmonett, A. C.; Pickard, F. C. t.; Shao, Y.; Cheatham, T. E., 3rd; Brooks, B. R. Efficient treatment of induced dipoles. *J. Chem. Phys.* **2015**, *143*, No. 074115.
(59) Sala, J.; Guardia, E.; Masia, M. The polarizable point dipoles method with electrostatic damping: implementation on a model system. *J. Chem. Phys.* **2010**, *133*, No. 234101.
(60) Case, D. A.; Darden, T. A.; Cheatham, I. T. E.; Simmerling, C. L.; Wang, J.; Duke, R. E.; Luo, R.; Walker, R. C.; Zhang, W.; Merz, K. M.; Roberts, B.; Hayik, S.; Roitberg, A.; Seabra, G.; Swails, J.; Götz, A. W.; Kolossváry, I.; Wong, K. F.; Paesani, F.; Vanicek, J.; Wolf, R. M.; Liu, J.; Wu, X.; Brozell, S. R.; Steinbrecher, T.; Gohlke, H.; Cai, Q.; Ye, X.; Wang, J.; Hsieh, M.-J.; Cui, G.; Roe, D. R.; Mathews, D. H.; Seetin, M. G.; Salomon-Ferrer, R.; Sagui, C.; Babin, V.; Luchko, T.; Gusarov, S.; Kovalenko, A.; Kollman, P. A. *AMBER 12*; University of California: San Francisco, 2012.
(61) Ryckaert, J.-P.; Ciccotti, G.; Berendsen, H. J. C. Numerical integration of the cartesian equations of motion of a system with constraints: molecular dynamics of n-alkanes. *J. Comput. Phys.* **1977**, *23*, 327−341.
(62) Darden, T.; York, D.; Pedersen, L. Particle mesh Ewald: AnN·log(N) method for Ewald sums in large systems. *J. Chem. Phys.* **1993**, *98*, 10089−10092.
(63) Berendsen, H. J. C.; Postma, J. P. M.; van Gunsteren, W. F.; DiNola, A.; Haak, J. R. Molecular dynamics with coupling to an external bath. *J. Chem. Phys.* **1984**, *81*, 3684−3690.
(64) Pastor, R. W.; Brooks, B. R.; Szabo, A. An analysis of the accuracy of Langevin and molecular dynamics algorithms. *Mol. Phys.* **1988**, *65*, 1409−1419.
(65) Tozer, D. J. Relationship between long-range charge-transfer excitation energy error and integer discontinuity in Kohn−Sham theory. *J. Chem. Phys.* **2003**, *119*, 12697−12699.
(66) Dreuw, A.; Weisman, J. L.; Head-Gordon, M. Long-range charge-transfer excited states in time-dependent density functional theory require non-local exchange. *J. Chem. Phys.* **2003**, *119*, 2943−2946.
(67) Perdew, J. P.; Zunger, A. Self-interaction correction to density-functional approximations for many-electron systems. *Phys. Rev. B* **1981**, *23*, 5048−5079.
(68) Aksu, H.; Schubert, A.; Geva, E.; Dunietz, B. D. Explaining Spectral Asymmetries and Excitonic Characters of the Core Pigment

https://dx.doi.org/10.1021/acs.jctc.0c00796
J. Chem. Theory Comput. 2020, 16, 6481−6490

Pairs in the Bacterial Reaction Center Using a Screened Range-Separated Hybrid Functional. *J. Phys. Chem. B* **2019**, *123*, 8970−8975.
(69) Sun, X.; Ladanyi, B. M.; Stratt, R. M. Effects of Electronic-State-Dependent Solute Polarizability: Application to Solute-Pump/Solvent-Probe Spectra. *J. Phys. Chem. B* **2015**, *119*, 9129−9139.
(70) Ohio Supercomputer Center. http://osc.edu/ark:/19495/f5s1ph73.

https://dx.doi.org/10.1021/acs.jctc.0c00796
J. Chem. Theory Comput. 2020, 16, 6481−6490